Reactive melt infiltration of carbon fibre reinforced ZrB2/B composites with Zr2Cu

Reactive melt infiltration of carbon fibre reinforced ZrB_2/B composites with Zr_2Cu

Antonio Vinci[1], Luca Zoli[1], Pietro Galizia[1], Marius Kütemeyer[2], Dietmar Koch[3], Diletta Sciti[1]

[1] *CNR-ISTEC, Institute of Science and Technology for Ceramics, Via Granarolo 64, I-48018 Faenza, Italy*

[2] *Spicetech GmbH, Schloßstraße 59 C, 70176 Stuttgart, Germany*

[3] *University of Augsburg, Institute for Materials Resource Management, Am Technologiezentrum 5, 86159 Augsburg, Germany*

Abstract

The microstructure and mechanical properties of carbon fibre reinforced ZrB_2 composites produced by slurry infiltration and consolidated by reactive melt infiltration were investigated. Fibres were preliminary infiltrated with ZrB_2/B slurries with varying ZrB_2/B ratios. Then the composites were infiltrated with Zr_2Cu melt at 1200°C under vacuum. Boron was chosen as the reactant phase, while raw ZrB_2 was added as a filler to prevent excessive swelling. With increase of boron content the infiltration becomes more difficult due to the reaction of alloy and boron. The boron is completely converted to nano ZrB_2 grains. Some ZrC is produced from the side reaction between Zr_2Cu and the carbon fibre, resulting in reduction of fibre diameter. The flexural strength increased from 360 to 560 MPa with the increase of boron content, while KIc amounted to 10 $MPa \cdot m^{0.5}$ but was affected by large scatter. The mechanical behaviour was mostly dominated by matrix properties.

Keywords

Ceramic-matrix composites (CMCs); Liquid metal infiltration; Microstructural analysis; Mechanical properties;

1. Introduction

The increasing demand for materials able to withstand extreme conditions and surpass the current state of the art C/C or C/SiC based CMCs has led to the design and development of a new class of CMCs based on a UHTC matrix, called UHTCMCs [1][2][3][4][5][6]. UHTCs are a class of materials characterized by

Corresponding author: antonio.vinci@istec.cnr.it

extremely high melting points and comprise the borides and carbides of early transition metals such as ZrB_2, HfB_2, ZrC, etc [7][8][9]. They possess high temperature strength, high thermal conductivity and good oxidation resistance when doped with silicon-containing additives and have been extensively investigated as candidates for the fabrication of reusable components for aerospace re-entry or hypersonic flight [10]. However their low fracture toughness and propensity to brittle fracture severely limits their application [11]. By substituting the ceramic matrix of conventional CMCs, based on silicon carbide which is not suitable above 1600°C, with a UHTC matrix, it is possible to maintain the high damage tolerance provided by the fibres and the high temperature resistance of UHTCs. Within the framework of the C^{3}harme project, these materials were tested and validated for the use in extreme environments [10][12]. Several routes have been explored for the fabrication of this novel class of materials:

- Radiofrequency assisted chemical vapour infiltration (RF-CVI) of carbon on a 2.5 D carbon preform impregnated with ZrB_2 or HfB_2 particles [13]
- Polymer infiltration and pyrolysis of carbon fibres with SiC precursors doped with UHTC particles, [14].
- Slurry infiltration of carbon fibres with ZrB_2/SiC based suspensions, followed by hot pressing or spark plasma sintering [4][5][15].

An alternative route for the fabrication of carbon fibre reinforced ZrB_2 composites is based on the slurry infiltration of a fibre preform with boron-containing powders (i.e. B, B_4C) followed by reactive melt infiltration (RMI) with liquid zirconium alloys. Typically, Zr_2Cu alloy is employed as liquid melt due to its lower melting point (~1000°C) compared to elemental zirconium (1855°C), to form in-situ ZrB_2 and Cu according to reaction 1:

$$4\ B + Zr_2Cu \rightarrow 2\ ZrB_2 + Cu \qquad (1)$$

This allows to obtain nearly full density materials without the need of high temperatures and pressures required for the conventional sintering of UHTCs. The main drawbacks of this process are linked to the powder wettability, which may hinder infiltration, and the presence of residual melt at the end of the infiltration which can lower the high temperature mechanical properties. Moreover, the formation of in-situ

Corresponding author: antonio.vinci@istec.cnr.it

ZrB_2 leads to a volume expansion which may choke infiltration at the reaction front or delaminate the composite.

In order to achieve the homogenous infiltration of the slurry infiltrated preform, a high degree of porosity and capillary forces are required, as well as a low contact angle between the reactive melt and the substrate. Previous studies on the wettability of Zr- alloys with different substrates reported low contact angles between ZrB_2 and Zr-Cu alloys [16], and contact angles below 90° on a carbon substrate at 1200°C [17]. Furthermore, the addition of 1% boron in the Zr_2Cu alloys allows to lower the melting temperature while still maintaining low contact angles with the substrates [17][18] [19]. It is essential to infiltrate a Si free preform in order to stay clear of Zr-Si phases and their large volume expansion.

In the present work carbon fibre reinforced ZrB_2/ZrC composites were fabricated via RMI. The use of a protective coating was intentionally avoided since the goal of this work was to study and limit the extent of reaction of the molten phase with the fibres [18]. Different compositions in terms of ZrB_2/B volumetric filler ratio were evaluated. Microstructure and mechanical properties were analysed and compared.

2. Experimental

2.1. Materials

For the preparation of ceramic slurries, the following powders were used: ZrB_2 powder (H.C. Starck, grade B, Germany, specific surface area 1.0 m^2/g, particle size range 0.5-6 µm, impurities (wt.%): 0.25 C, 2 O, 0.25 N, 0.1 Fe, 0.2 Hf), elemental Boron 95% (TRADIUM GmbH, Germany, particle size 1.08 µm, impurities (wt.%): 0.30 Mg, 0.12 H_2O, 0.25 $B(OH)_3$, 0.91 H_2O_2), Zr_2Cu (Additional alloying element: 1% boron, HMW Hauner GmbH & Co. KG). Unidirectional Ultra-High modulus carbon fibre cloths were chosen for the infiltration processes (Granoc, XN80-6K fibres; tensile modulus 780 GPa, tensile strength 3.4 GPa, Ø = 10 µm, supplier: G. Angeloni).

2.2 Process

Aqueous powder suspensions containing elemental boron and commercial zirconium diboride in varying ratios were prepared following the procedures described in previous works [20]. With these slurries,

Corresponding author: antonio.vinci@istec.cnr.it

unidirectional fibre fabrics of dimensions 50 × 50 mm were infiltrated, stacked in a unidirectional configuration and then dried at 100°C in an oven. The ratio between the fibre and the ceramic powder volumetric amount was maintained at 1:1 for all compositions by adjusting the slurry rheology. Composites were labelled based on the powder compositions: B25 (25% B, 75% ZrB_2 vol), B50 (50% B, 50% ZrB_2 vol), B75 (75% B, 25% ZrB_2 vol). Then the green bodies were clamped between two graphite plates and attached to a sample holder by a screw inside a furnace, while the Zr_2Cu powder was placed in a graphite crucible at the bottom of the furnace: the furnace was heated to 1200°C at a rate of 500°C/h in argon atmosphere in order to melt the Zr_2Cu without causing bubbling of the melt. Once the target temperature was reached, the chamber was evacuated to a pressure < 5 mbar and the sample was submerged in the melt for 2 min at half height and then taken out. After the RMI process, the chamber was cooled down to a rate of 300°C/h. Sample B75 required a second infiltration cycle due to excessive volume expansion from the formation of in-situ ZrB_2 and premature halt of the infiltration at the reaction front. The process is illustrated in figure 1.

Corresponding author: antonio.vinci@istec.cnr.it

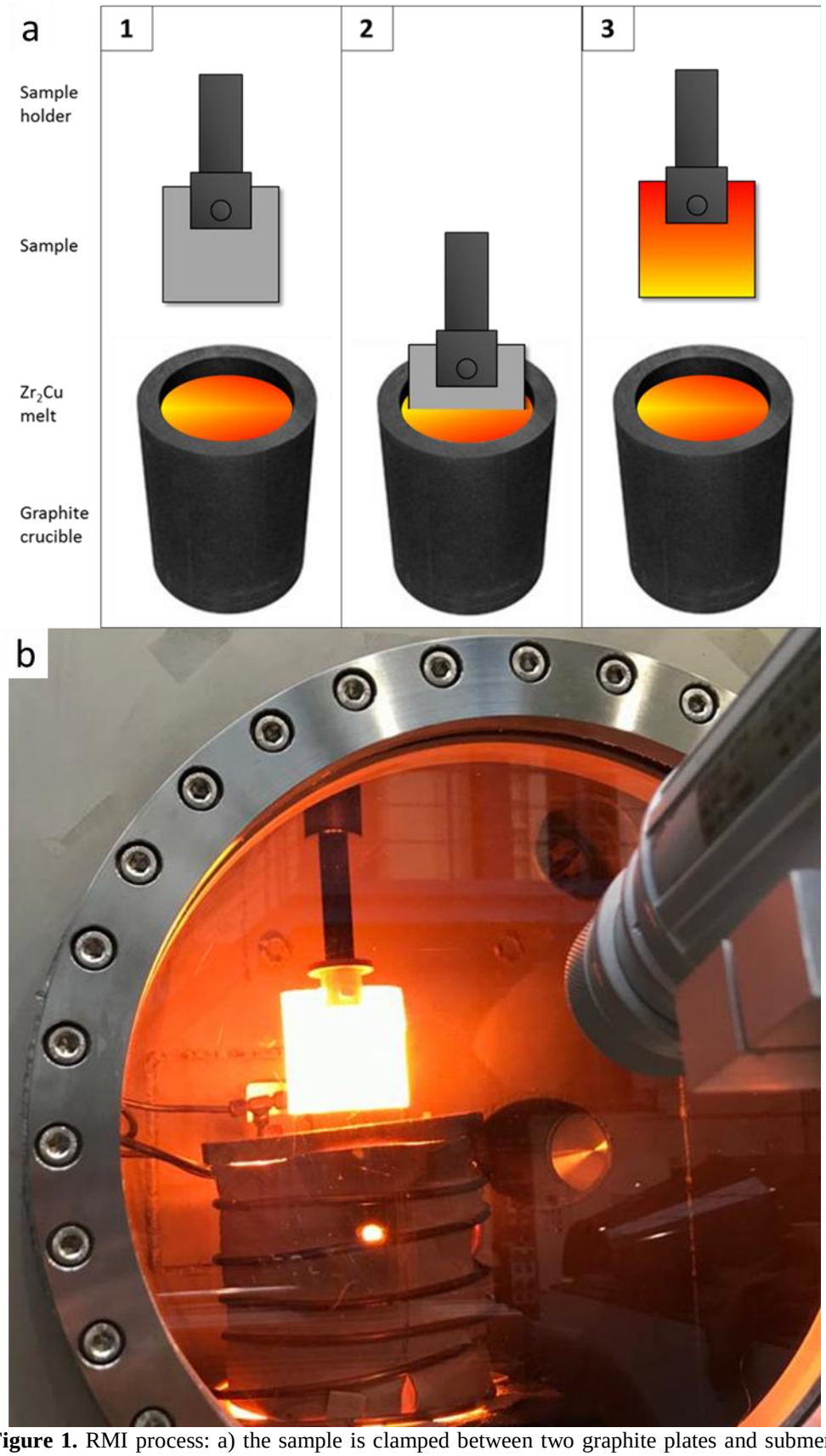

Figure 1. RMI process: a) the sample is clamped between two graphite plates and submerged at half height inside the Zr_2Cu melt. After 2 min, the melt has infiltrated the entire sample. b) Picture of the sample infiltrated with the reactive melt

Corresponding author: antonio.vinci@istec.cnr.it

2.3. Microstructure analysis

The composites microstructure was analysed on polished and fractured surfaces by field emission scanning electron microscopy (FE-SEM, Carl Zeiss Ultra 55 Plus, Germany) and energy dispersive X-ray spectroscopy (EDX, AZtec, Oxford instruments, UK). Samples for microscopy were polished down to a 0.25 μm finish with diamond abrasives using a semi-automatic polishing machine. The polished samples were then washed with ethanol in an ultrasonic bath for 5 min up to 3 times and then dried for 1h at 80°C in an oven. The slurry infiltrated carbon preform had a nominal porosity of 40%, determined as geometric porosity. Taking into account a fibre/matrix ratio of 1:1, the initial fibre amounts for all specimens was ~35%. The final fibre volumetric amount after RMI was measured by image analysis on the polished surfaces of the samples with software Image Pro Analyser 7.0. The composition and phases formed after RMI were also analysed by X-ray diffraction analysis (Bruker AXS D8 with Cu Kα (λ = 154 pm), Germany). The final density was measured through the geometrical method.

2.4. Mechanical properties

Flexural strength was evaluated by four-point bending on specimens 25 mm × 2.5 mm × 2 mm in size using a fully articulated steel fixture having a lower span of 20 mm and an upper span of 10 mm and at a cross-head rate of 1 mm/min, following the guidelines of standard ISO 14704:2016 (EN). Even though for fibre reinforced composites a high span/thickness ratio is typically advised, the available material was not enough to fabricate larger specimens. Flexural strength was evaluated along the fibre orientation to better understand the contribution provided by the fibre reinforcement. Fracture toughness (K_{Ic}) was evaluated by four-points chevron notch bending tests (CNB) following standard ASTM C1421. The specimens were 25 mm × 2 mm × 2.5 mm^3 (length × width × thickness) and were notched with a 0.1 mm-thick diamond saw. The chevron-notch tip depth and average side length were about 0.12 and 0.80 of the bar thickness, respectively. The crosshead speed was 0.05 mm/min. The "slice model" equation of Munz et al. [33] was used to calculate K_{Ic}.

Corresponding author: antonio.vinci@istec.cnr.it

3. Results and discussion

3.1 Microstructure of the sintered material

Microstructural features of the materials fabricated are reported in Table 1. All composites were fully dense, with densities ranging between 6.1 g/cm^3 and 6.6 g/cm^3. The final fibre volumetric amounts were lower than the starting ones due to sample swelling and fibre degradation. The grain size of ZrB_2 filler increased slightly with the increase of boron content, but was still comparable with the starting size of the powders.

Table 1. Values of bulk density, porosity, fibre content, ZrC content and ZrB_2 particle size (from powders and RMI respectively)

Sample	Density (g/cm^3)	Porosity (vol%)	Fibre volume after RMI (vol%)	ZrB_2 grain size powders (μm)	ZrB_2 grain size RMI (nm)
B25	6.36	< 1	13.4 ± 0.4	2.30	140
B50	6.64	< 1	16.5 ± 1.4	2.45	170
B75	6.12	< 1	24.7 ± 4.5	3.00	290

X-Ray diffraction analysis was carried out on the polished cross section of sample B25 (Fig. 2), used as reference. The main peaks were indexed to ZrB_2 (PDF#34-0423) and ZrC (PDF#65-0973). Only one ZrB_2 phase was revealed, suggesting that the in-situ ZrB_2 had the same structure of the one already present in the form of powders. No carbon was detected, while intense peaks from ZrC originating from carbon consumption were observed. Smaller peaks were attributed to the residual melt alloy Zr-Cu.

Corresponding author: antonio.vinci@istec.cnr.it

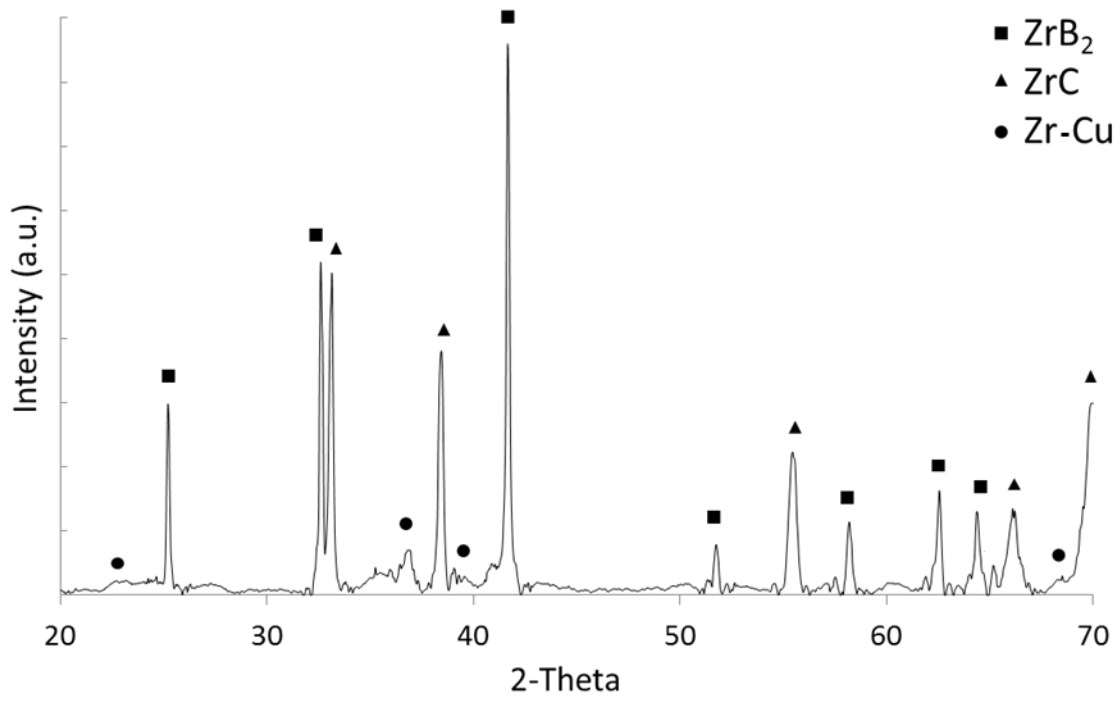

Figure 2. X-Ray diffraction pattern on the polished cross section of sample B25 after infiltration with Zr_2Cu. The phases detected were ZrB2 (PDF#34-0423), ZrC (PDF#65-0973) and the leftover alloy Zr-Cu.

All specimens were characterized by very similar microstructure. As an example, the low magnification micrograph of sample B25 is reported in figure 3.

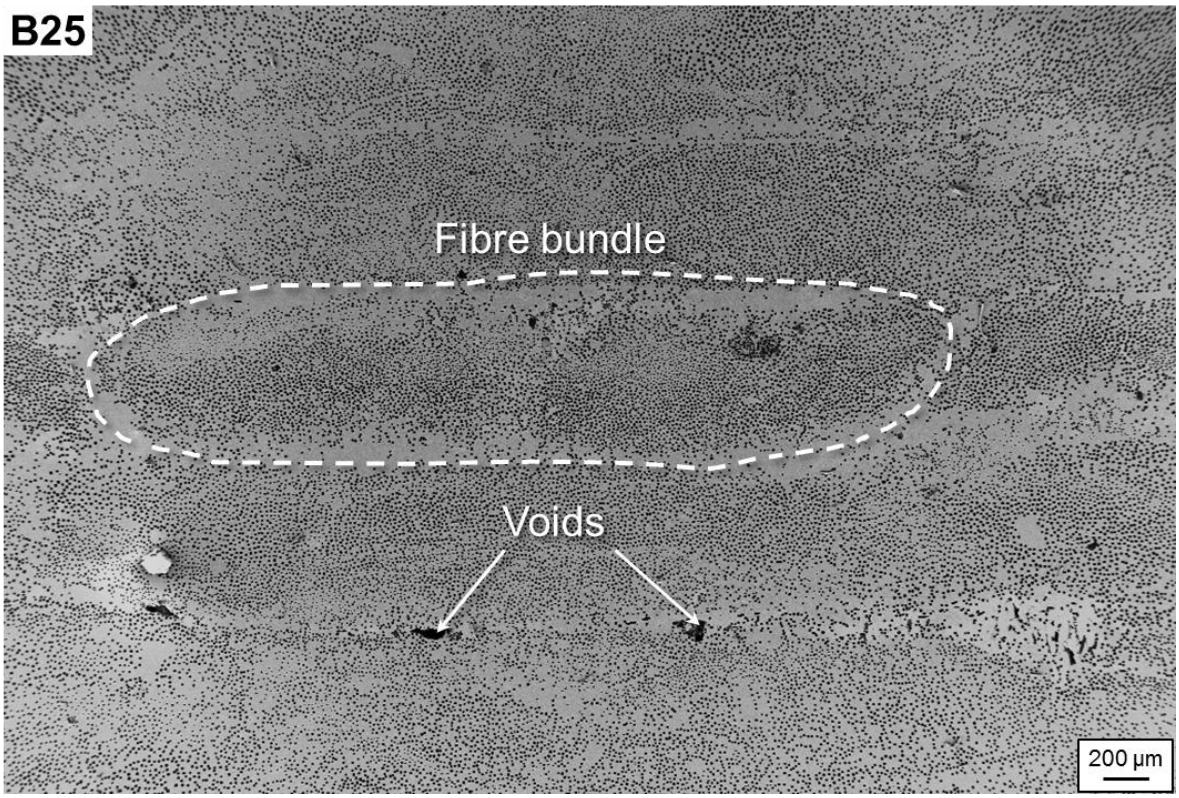

Corresponding author: antonio.vinci@istec.cnr.it

Figure 3. Low magnification micrograph of sample B25 showing the fibre distribution in the ceramic matrix and the most common defects (voids) between layers.

All samples underwent due to RMI swelling and were covered with residual Zr_2Cu that was machined off. The microstructures were almost flawless with sporadic voids between fibre bundles or between layers due to incomplete infiltration. The fibres were homogeneously distributed in the ceramic matrix for all samples. SEM micrographs in figure 4 show the typical fiber distribution and the fiber/matrix interface. For all the samples the final fibre content measured by image analysis (Table 1) was much lower than the initial ones: 13, 17, 25% for B25, B50 and B75 respectively, and this was reflected in the high densities of the specimens. There are two main explanations to this phenomenon:

1) the starting fibre volumetric amount in the slurry infiltrated preform, taking into account a porosity of 40%, was ~35 vol%; since the specimens experienced a volume expansion, due to the formation of ZrB_2 and ZrC, of up to ~30% during RMI, the final fibre content, normalized on the final composite volume, was lower (25 – 30%)

2) a large fraction of the fibres reacted with the surrounding Zr_2Cu melt leading to the formation of ZrC at the interface, further lowering the final carbon fibre content.

All samples contained large amounts of unreacted melt which contributed to increase the final density of the materials., essentially filling the voids in between the ZrB2 and ZrC grains. Earlier attempts aimed at reducing the final residual melt amount resulted in incomplete infiltration.

Corresponding author: antonio.vinci@istec.cnr.it

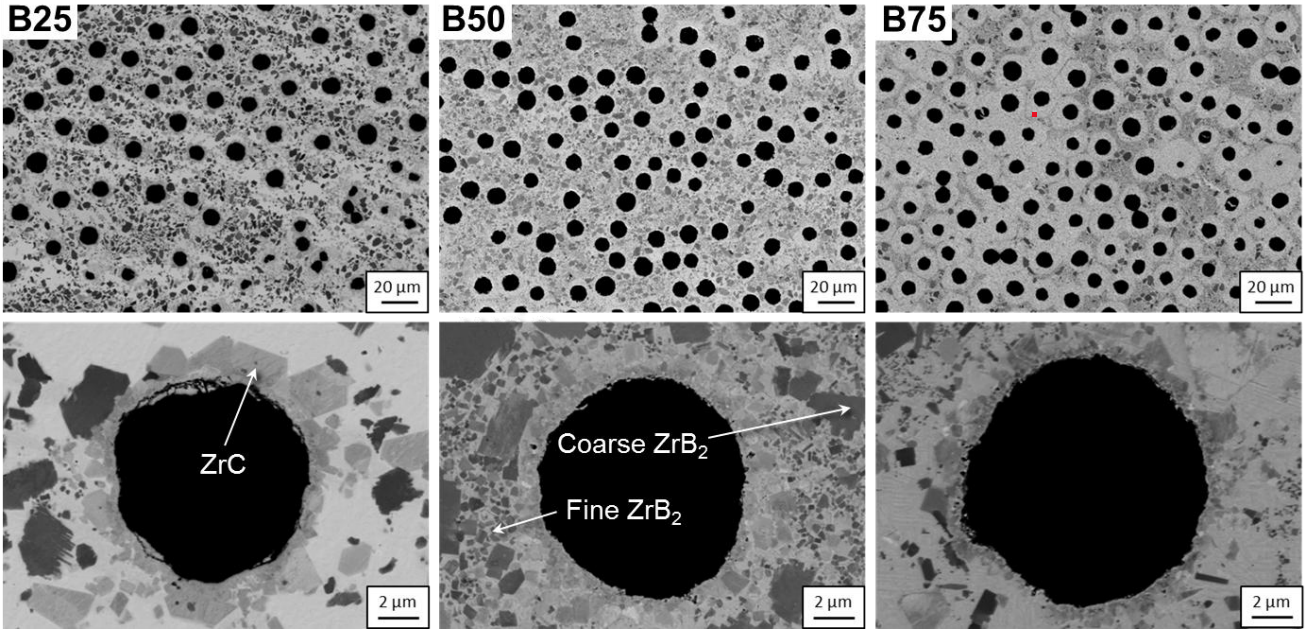

Figure 4. SEM image of the polished cross section of samples B25, B50 and B75. The black phase is carbon from the fibres, dark grey and light grey phases are ZrB_2 and ZrC respectively while the white phase is the residual Zr_2Cu melt.

The microstructure of B50 was very similar to that of B75. Cubic ZrC grew on the surface of the fibres as the latter reacted with the melt. Fibre-dense regions were affected by fibre degradation to a lesser degree, whereas less infiltrated peripheral fibres were almost completely converted into ZrC. This effect was previously observed on ZrB_2/SiC composites obtained by sintering, in which peripheral fibres surrounded by large amount of ceramic matrix would often show strong signs of reaction [6].

Fibres were surrounded by a rim of ZrC which originated from the reaction between the carbon of the fibre and the liquid melt according to the reaction 1. In order to quantify the degree of fibre consumption, the fibre diameter distribution was evaluated by image analysis and compared with a standard sample containing the same fibres in a SiC matrix obtained by PIP (figure 5). The mean diameter of the fibres used in this work, XN80, was 10 µm. For sample B25, a bimodal distribution of fibres diameter was observed, with mean diameters of 6.7 µm and 10 µm respectively. This was attributed to the inhomogeneity of the sample that was characterized by fibre dense regions where fibres retained their size, and matrix dense regions where most fibres reacted. This measurement was likely overestimated because it was not possible to detect those fibres that were completely converted into ZrC. For samples B50 and B75 the degree of fibre degradation was lower. These samples were characterised by mean fibre diameters of 9.3 µm and 8.6 µm respectively, indicating that

Corresponding author: antonio.vinci@istec.cnr.it

up to 19% of the fibre was consumed in the process. B25 was the most affected by it because it also had a very high content of unreacted melt. On the other hand, B50 and B75 were very similar in this regard. The reason why B75 showed a slightly higher degree of fibre degradation could be attributed to the higher amount of energy generated from the exothermic reaction of boron with the reactive melt. The second infiltration might also have contributed. Even though B50 was characterized by the lowest degree of reaction, B75 retained the highest fibre content (table 1). This was attributed to the higher extent of swelling after RMI for B50 compared to B75 and the higher amount of unreacted alloy in the matrix that contributed to further lowering the fibre content and increase the density. On the other hand, the infiltration of B75 was much more difficult because the infiltration process would come to an early halt, and not much residual alloy would be left over. Theoretically, the higher the boron content, the higher the volume expansion from the formation of new ZrB_2. However, with the increase of boron, infiltration also becomes more difficult. The result is that the majority of the swelling was mostly due to the melt infiltrating the sample and spreading the fibres. While infiltration was easy for B25 and B50 (higher melt mobility and lower viscosity because of medium/low amount of boron), it was very difficult for B75, which was the least subjected to swelling as it was barely infiltrated and required a 2nd infiltration that still did not lead to full material infiltration. Only 3 cm of material were infiltrated, while for B25 and B50 it was possible to infiltrate up to 5 cm.

Corresponding author: antonio.vinci@istec.cnr.it

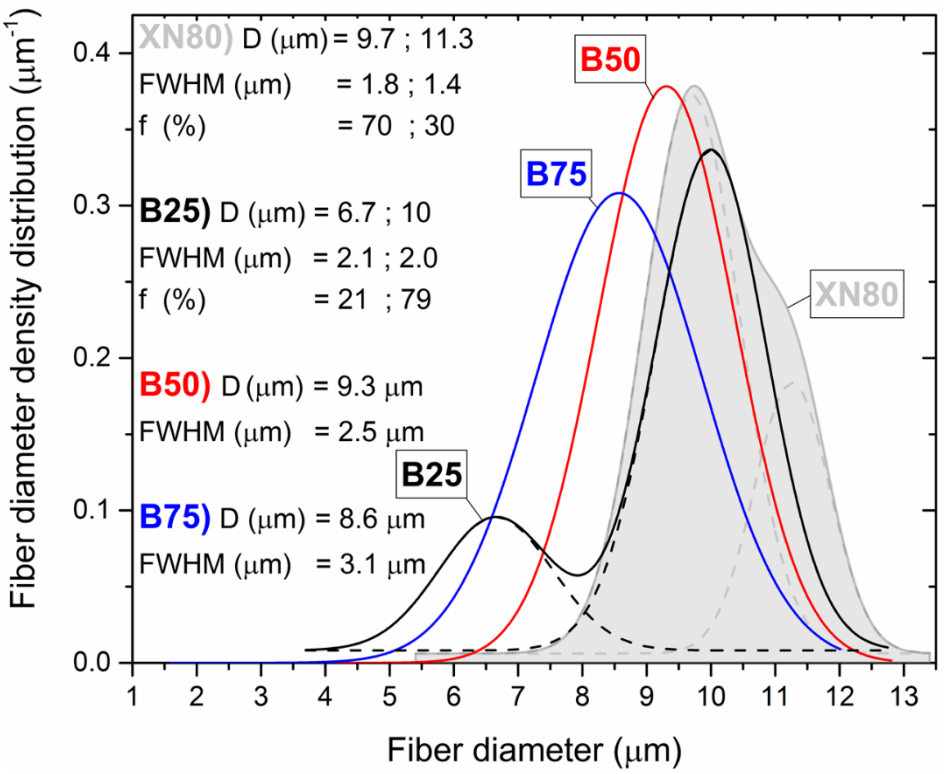

Figure 5. Mean fibre diameter distribution for a standard sample obtained by PIP where fibres were unreacted (XN80), compared to the samples obtained by RMI, B25, B50 and B75. For XN80 and B25, a bimodal distribution was observed.

From SEM-EDS analysis on the specimens after RMI (figure 6), two types of ZrB_2 phases were identified: large grains (2 – 3 μm) came from the starting commercial powders that were used as a filler, while the fine grains (< 300 nm) originated from the reaction between boron and the reactive melt and were homogeneously dispersed in the Zr-Cu alloy. These small particles had very well defined borders and geometries and were often found as closely packed clusters. These are very typical of cermets obtained by RMI or reactive hot pressing, where the small reactant particles react with the melt and give rise to the formation of these plate-like crystals [21][22][23].

Corresponding author: antonio.vinci@istec.cnr.it

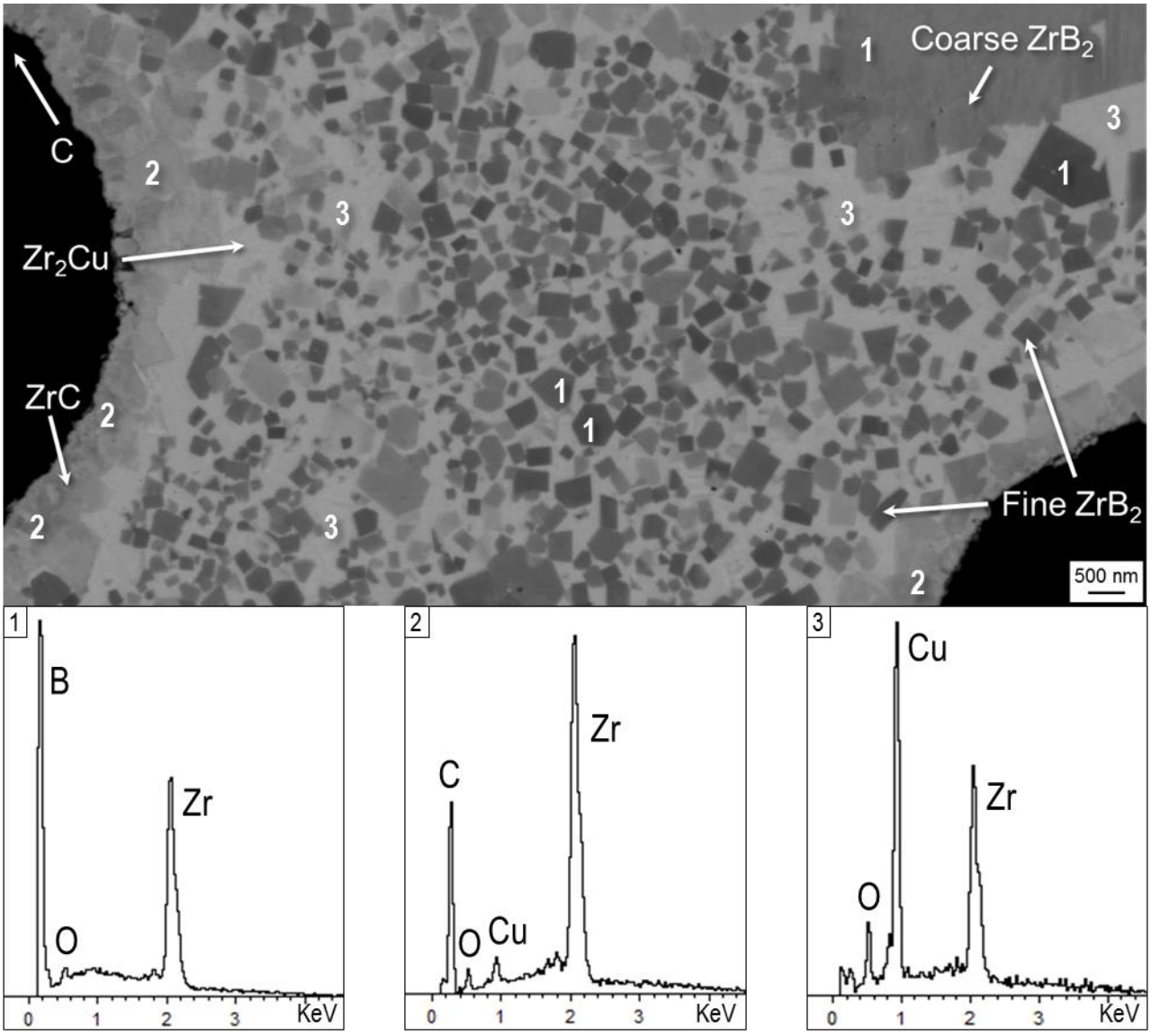

Figure 6. Detail of the microstructure of B75 showing the ZrC rim around fibres, coarse ZrB_2 from the starting powders (filler) and the fine grained ZrB_2 originating from the reaction between elemental boron and Zr_2Cu melt and the respective EDX spectra below.

The volumetric fraction of the fine ZrB_2 particles increased with the increase of boron content in the starting powders, while no residual boron was observed. This was expected as the higher the starting boron content, the higher the resulting ZrB_2. Small amounts of oxygen were detected from EDX analysis (figure 6); these could be attributed to oxide impurities already present in the starting powders or the oxidation of boron with water during the preparation of the ceramic slurries. Upon further inspection of the microstructure of the ceramic matrix, it was found that the majority of coarse ZrB_2 particles from powders did not retain their

Corresponding author: antonio.vinci@istec.cnr.it

original shape but were characterized by a peculiar jagged surface, resembling the phenomenon of grain twinning typically observed in minerals (figure 7). The degree of "jaggedness" was more pronounced in the case of B25, where the branches would reach a length equal or superior to the original grain dimension. With the increase of boron content, the irregularity and the branches length decreased, while the ZrB_2 grains appeared larger. Moreover, the branches extending from the ZrB_2 particles were perfectly parallel to each other. It is hypothesized that a fraction of the ZrB_2 formed by RMI with the Zr_2Cu melt nucleated on the surface of the already present ZrB_2 particles from the powders, and grew preferentially along specific planes. It could also be speculated that in the case of B25, due to the lower amount of available boron, boron particles had a higher mobility in the melt and could more easily dissolve and precipitate as ZrB_2 crystals on the already present ZrB_2 particles and grow continuously along preferential planes. Finally, the increase in size with increasing boron content could be attributed to the larger amount of fine ZrB_2 that grew on the starting ZrB_2 grains from powders.

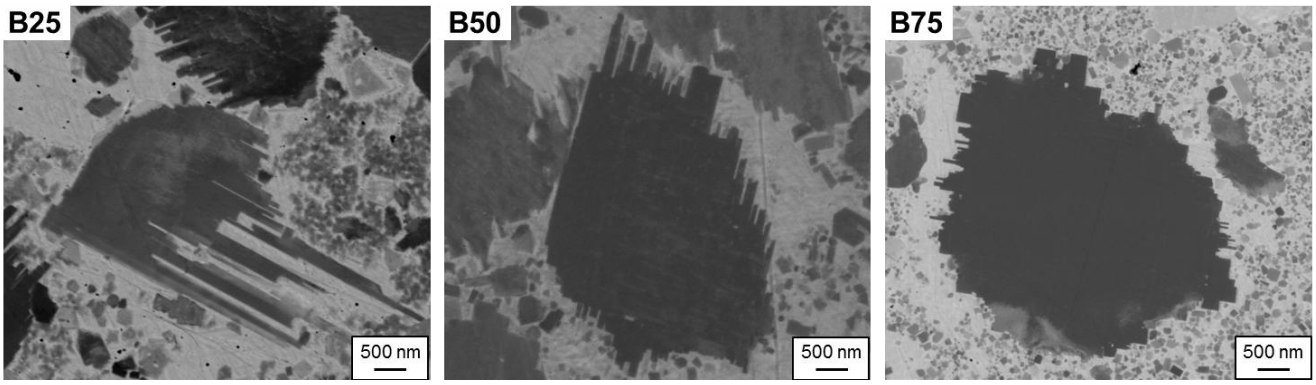

Figure 7. Detail of the jagged ZrB_2 grains. The dark and light grey phase represents ZrB_2 and Zr_2Cu respectively. ZrB_2 grain size increases with the increase of boron content.

3.2 Mechanical properties

The values of flexural strength and fracture toughness are reported in table 2. For sample B75 it was not possible to produce bars for fracture toughness testing because the infiltration came to a premature halt and there was not enough available material in spite of the second infiltration.

Corresponding author: antonio.vinci@istec.cnr.it

Table 2. Values of flexural strength and fracture toughness along the fibre orientation. Fibre vol% is reported.

Sample	Fibre volume after RMI (vol%)	Flexural Strength (MPa)	Fracture Toughness 0° ($MPa \cdot m^{0.5}$)
B25	13.4 ± 0.4	332 ± 15	10.9 ± 0.6
B50	16.5 ± 1.4	452 ± 255	9.2 ± 6.5
B75	24.7 ± 4.5	563 ± 29	-

All specimens fracture in a predominantly brittle mode (figure 8); this was attributed to the predominantly ceramic nature of these materials due to the low fibre content. The higher strength of B50 and B75 compared to B25 could be attributed to the higher amount of fine ZrB_2 particles in the metal matrix that provide a better particle reinforcement. The highest strength was obtained for B75, which was also the most difficult to infiltrate. These materials displayed higher values of strength and toughness compared to those reported for 97% dense ZrB_2/ZrC cermets obtained via RMI at 1200°C [24], while they are comparable to ZrB_2-ZrC-Zr cermets obtained via reactive hot pressing [21][25][26], but were characterized by a lower density because of the presence of carbon fibres.

Sample B50 was affected by large data scatter. This was attributed to process-induced flaws in the specimen that resulted in premature failure of some bars during testing.

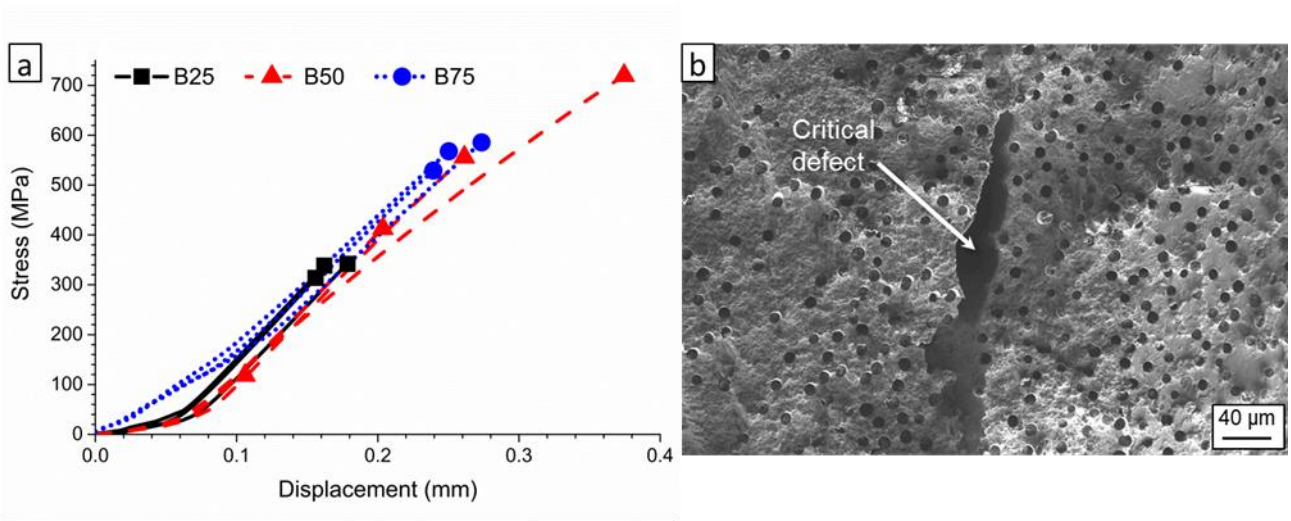

Figure 8. a) Stress/displacement curves for samples B25, B50 and B75. b) fracture surface of one of B50 bars which shows a large flaw in the material that resulted in premature failure of the specimen.

Corresponding author: antonio.vinci@istec.cnr.it

The fracture surface (Fig. 8b and fig. 9a, b) was typically characterized by very short fibre pull-out (< 5 μm) and was more similar to that of conventional ceramics. Compared to sintered fibre reinforced ZrB_2/SiC composites previously studied by the same authors, the strength reported for these materials is roughly 50% higher because they did not suffer interlaminar shear and gave a valid bending failure under tensile stress. Fracture toughness is comparable, in spite of the low fibre amount. The relatively high fracture toughness of these composites could be attributed to the partly metallic nature of the material rather than the fibre reinforcement. The jagged grains observed in figure 7 might also play a role. Looking at the detail of the fracture surface, it was observed that the ZrC rim around fibres was actually detached from the fibre (fig. 9d). This could be attributed to the shrinkage of the metallic phase during cooling that led to the fibre/matrix debonding and suggested that fibres were not strongly involved in the strengthening and toughening mechanisms. In support of this it can be noted that a relevant amount of fibres close to the fractured matrix surface displayed little to no pull-out, even though the fibre/matrix interface was supposedly weak; this suggested a matrix dominated behaviour in these composites which was accompanied by a large energy release during crack propagation, see the brittle failure of Figure 8. The relative high values of "K_{Ic}" could be overestimated because the plain strain condition would have not been guaranteed. In fact, the value of $2.5(K_I/\sigma)^2$ may have been greater than the specimen thickness and crack length. Hence further experiments with larger specimens are necessary to confirm if the measured K_I was the critical stress intensity factor.

Corresponding author: antonio.vinci@istec.cnr.it

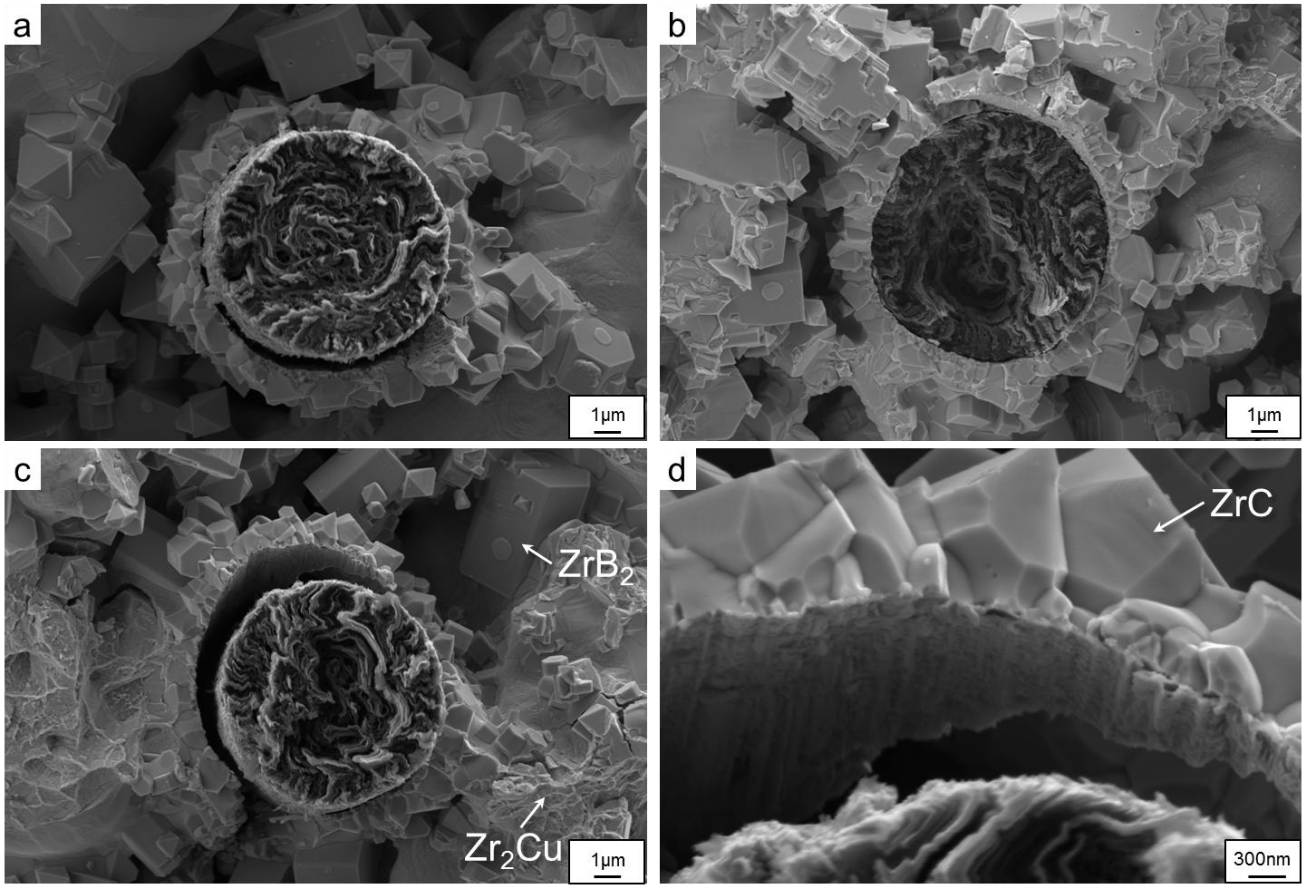

Figure 9. Fracture surface of samples B25 - B75: a) fibre surrounded by a ZrC rim in a hollow, b) typical fibre fracture surface, c) fibre detached from the ZrC rim, d) detail of the fibre/matrix interface

The fractured ceramic matrix was further investigated in order to find and study the behaviour of the jagged ZrB_2 grains previously observed in the microstructure (Fig. 10). The branches protruding from the ZrB_2 grain extended for the whole depth of the grain and gave origin to a terraced fracture. It is unclear whether these particles played a toughening role during fracture, as the grain itself showed brittle fracture, but the branches interlocked well with the surrounding residual melt and anchored the grain to the matrix.

Corresponding author: antonio.vinci@istec.cnr.it

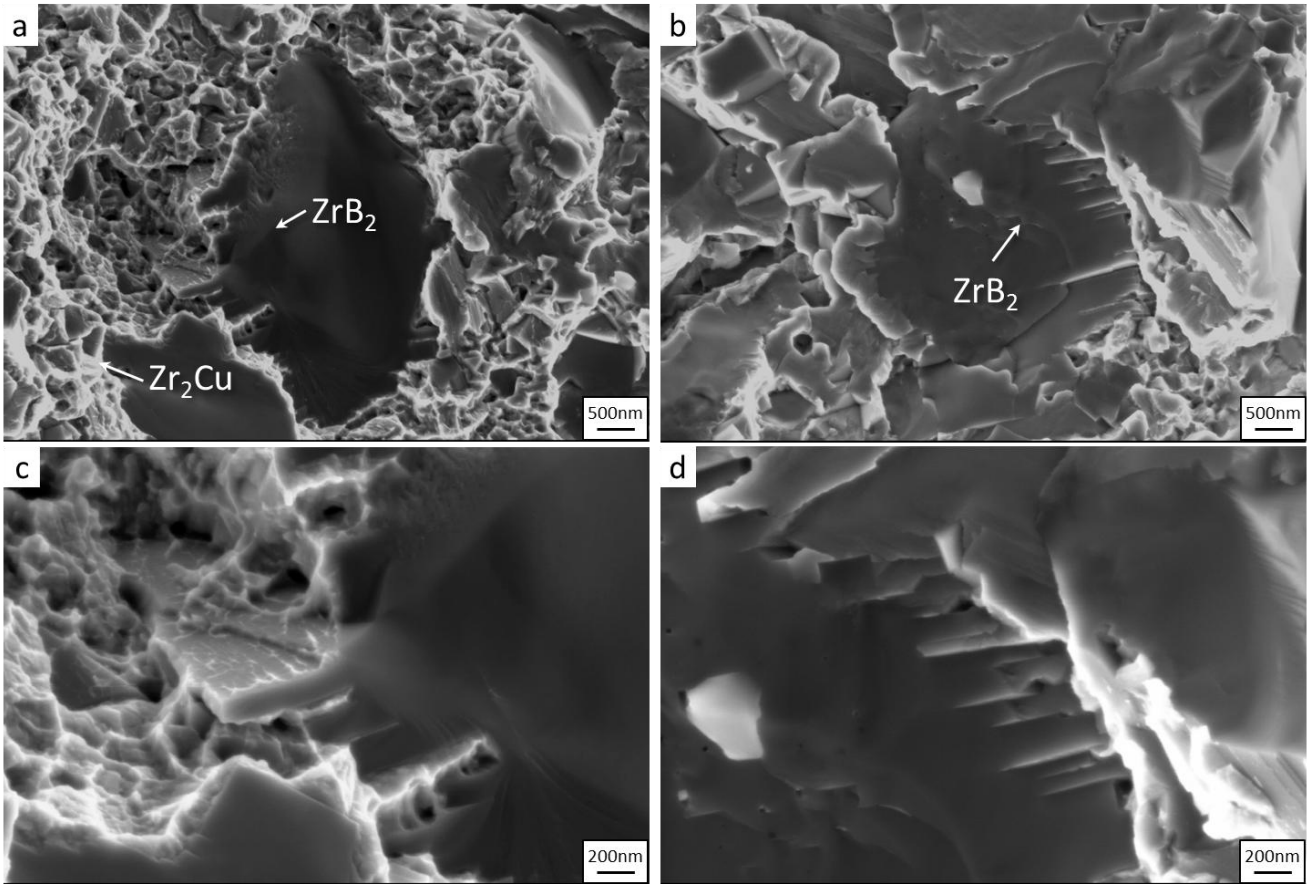

Figure 10. Fracture surface of the ceramic matrix showing the jagged ZrB_2 grains and the terraced fracture with the branches of the grains interlocking with the metallic matrix.

Conclusions

A new processing route for the fabrication of fibre reinforced UHTCs was investigated. Carbon fibre preforms containing B/ZrB_2 mixtures in varying ratios were infiltrated with Zr_2Cu melt at 1200°C. All specimens were nearly fully dense and were characterized by < 1% porosity. The microstructure was characterized by coarse ZrB_2 from the commercial powders and fine ZrB_2 particles originating from the reaction between B and Zr_2Cu embedded in a matrix of Zr_2Cu. Increasing the boron content in the starting powders led to an increase of the fine ZrB_2 grains fraction originating from RMI. Sample B50 is characterized by the lowest degree of fibre degradation but also by a higher amount of residual melt that ultimately lowers the final fibre content and contributes to increase density. The strength of the composites is in the range of 350 – 560 MPa, with the highest values obtained for B50 and B75. This was attributed to a higher volumetric fraction of the fine ZrB_2 that provided better reinforcement. All specimens failed catastrophically and the fracture surface was

Corresponding author: antonio.vinci@istec.cnr.it

characterized by minimal fibre pull-out, indicating that RMI samples behave more like cermet materials and the mechanical behaviour is dominated by the matrix. Future works will be aimed at limiting the amount of unreacted alloy phase and investigate the role of the jagged grains more in depth.

Acknowledgements

This work has received funding from the European Union's Horizon 2020 "Research and innovation programme" under grant agreement N°685594 (C^3HARME). We wish to thank Cesare Melandri from ISTEC for mechanical testing. The authors also wish to thank German Aerospace Center DLR, Institute of Structures and Design, Stuttgart, for providing lab and furnace for RMI and Stefan Frick from DLR for running the RMI cycles.

- The raw/processed data required to reproduce these findings cannot be shared at this time due to technical or time limitations.

References

[1] Rueschhoff LM, Carney CM, Apostolov ZD, Cinibulk MK. Processing of fiber-reinforced ultra-high temperature ceramic composites: A review. International Journal of Ceramic Engineering & Science 2020;2:22–37. doi:10.1002/ces2.10033.

[2] Sciti D, Silvestroni L, Monteverde F, Vinci A, Zoli L. Introduction to H2020 project C3HARME–next generation ceramic composites for combustion harsh environment and space. Advances in Applied Ceramics 2018. doi:10.1080/17436753.2018.1509822.

[3] Zoli L, Sciti D. Efficacy of a ZrB2–SiC matrix in protecting C fibres from oxidation in novel UHTCMC materials. Materials & Design 2017;113:207–13. doi:10.1016/j.matdes.2016.09.104.

[4] Vinci A, Zoli L, Sciti D, Melandri C, Guicciardi S. Understanding the mechanical properties of novel UHTCMCs through random forest and regression tree analysis. Materials and Design 2018;145:97–107. doi:10.1016/j.matdes.2018.02.061.

[5] Zoli L, Vinci A, Galizia P, Gutièrrez-Gonzalez CF, Rivera S, Sciti D. Is spark plasma sintering suitable for the densification of continuous carbon fibre - UHTCMCs? Journal of the European Ceramic

Corresponding author: antonio.vinci@istec.cnr.it

Society 2019. doi:https://doi.org/10.1016/j.jeurceramsoc.2019.12.004.

[6] Galizia P, Failla S, Zoli L, Sciti D. Tough salami-inspired Cf/ZrB2 UHTCMCs produced by electrophoretic deposition. Journal of the European Ceramic Society 2018;38:403–9. doi:10.1016/J.JEURCERAMSOC.2017.09.047.

[7] A. Paul, D.D. Jayaseelan, S. Venugopal, E. Zapata-Solvas, J. Binner, B. Vaidhyanathan, A. Heaton, P. Brown WEL, UHTC. UHTC-composites for hypersonic applications. American Ceramic Society Bulletin 2012;91:22.

[8] Fahrenholtz WG, Hilmas GE, Talmy IG, Zaykoski JA. Refractory diborides of zirconium and hafnium. Journal of the American Ceramic Society 2007;90:1347–64. doi:10.1111/j.1551-2916.2007.01583.x.

[9] Fahrenholtz WG, Wuchina EJ, Lee WE, Zhou Y, editors. Ultra-High Temperature Ceramics: Materials for Extreme Environment Applications. Hoboken, New Jersey: John Wiley & Sons Inc.; 2014. doi:10.1002/9781118700853.

[10] Mungiguerra S, Di Martino GD, Savino R, Zoli L, Sciti D, Lagos MA. Ultra-High-Temperature Ceramic Matrix Composites in Hybrid Rocket Propulsion Environment. 2018 International Energy Conversion Engineering Conference, American Institute of Aeronautics and Astronautics; 2018. doi:doi:10.2514/6.2018-4694.

[11] Opeka MM, Talmy IG, Wuchina EJ, Zaykoski J a., Causey SJ. Mechanical, Thermal, and Oxidation Properties of Refractory Hafnium and zirconium Compounds. Journal of the European Ceramic Society 1999;19:2405–14. doi:10.1016/S0955-2219(99)00129-6.

[12] Mungiguerra S, Martino GD Di, Cecere A, Savino R, Silvestroni L, Vinci A, et al. Arc-jet wind tunnel characterization of ultra-high-temperature ceramic matrix composites. Corrosion Science 2019;149:18–28. doi:https://doi.org/10.1016/j.corsci.2018.12.039.

[13] Rubio V, Ramanujam P, Binner J. Ultra-high temperature ceramic composite. Advances in Applied Ceramics 2018;117:s56–61. doi:10.1080/17436753.2018.1475140.

[14] Uhlmann F, Wilhelmi C, Schmidt-Wimmer S, Beyer S, Badini C, Padovano E. Preparation and characterization of ZrB2 and TaC containing Cf/SiC composites via Polymer-Infiltration-Pyrolysis process. Journal of the European Ceramic Society 2017;37:1955–60. doi:10.1016/j.jeurceramsoc.2016.12.048.

Corresponding author: antonio.vinci@istec.cnr.it

[15] Vinci A, Zoli L, Landi E, Sciti D. Oxidation behaviour of a continuous carbon fibre reinforced ZrB<inf>2</inf>–SiC composite. Corrosion Science 2017;123. doi:10.1016/j.corsci.2017.04.012.

[16] Muolo ML, Ferrera E, Novakovic R, Passerone A. Wettability of zirconium diboride ceramics by Ag, Cu and their alloys with Zr. Scripta Materialia 2003;48:191–6. doi:https://doi.org/10.1016/S1359-6462(02)00361-5.

[17] Kütemeyer M, Schomer L, Helmreich T, Rosiwal S, Koch D. Fabrication of ultra high temperature ceramic matrix composites using a reactive melt infiltration process. Journal of the European Ceramic Society 2016. doi:10.1016/j.jeurceramsoc.2016.04.039.

[18] Kütemeyer M, Helmreich T, Rosiwal S, Koch D. Influence of zirconium-based alloys on manufacturing and mechanical properties of ultra high temperature ceramic matrix composites. Advances in Applied Ceramics 2018;117:s62–9. doi:10.1080/17436753.2018.1509810.

[19] Kütemeyer M, Shandler D, Koch D, Friess M. Reactive Melt Infiltration of Boron Containing Fiber Reinforced Preforms Forming a ZrB2 Matrix. Processing and Properties of Advanced Ceramics and Composites VII, John Wiley & Sons, Ltd; 2015, p. 169–80. doi:10.1002/9781119183860.ch18.

[20] Vinci A, Zoli L, Sciti D, Melandri C, Guicciardi S. Understanding the mechanical properties of novel UHTCMCs through random forest and regression tree analysis. Materials and Design 2018;145. doi:10.1016/j.matdes.2018.02.061.

[21] Guo S. Densification, microstructure, elastic and mechanical properties of reactive hot-pressed ZrB2–ZrC–Zr cermets. Journal of the European Ceramic Society 2014;34:621–32. doi:https://doi.org/10.1016/j.jeurceramsoc.2013.09.002.

[22] Tarraste M, Juhani K, Pirso J, Viljus M. Reactive Sintering of Bimodal WC-Co Hardmetals. Materials Science Medziagotyra 2015;21. doi:10.5755/j01.ms.21.3.7511.

[23] García J, Ciprés] V [Collado, Blomqvist A, Kaplan B. Cemented carbide microstructures: a review. International Journal of Refractory Metals and Hard Materials 2019;80:40–68. doi:https://doi.org/10.1016/j.ijrmhm.2018.12.004.

[24] Zhang S, Wang S, Li W, Zhu Y, Chen Z. Preparation of ZrB2 based composites by reactive melt infiltration at relative low temperature. Materials Letters 2011;65:2910–2. doi:10.1016/j.matlet.2011.06.070.

Corresponding author: antonio.vinci@istec.cnr.it

[25] Guo S. Textured microstructure and anisotropic strength of hot-forged ZrB2–ZrC–Zr cermets. Ceramics International 2016;42:16063–70. doi:https://doi.org/10.1016/j.ceramint.2016.07.116.

[26] Zhang S, Wang S, Li W, Zhu Y, Chen Z. Preparation of ZrB2 based composites by reactive melt infiltration at relative low temperature. Materials Letters 2011;65:2910–2. doi:https://doi.org/10.1016/j.matlet.2011.06.070.

Corresponding author: antonio.vinci@istec.cnr.it